

Journal of Materials Chemistry A

Accepted Manuscript



This is an *Accepted Manuscript*, which has been through the Royal Society of Chemistry peer review process and has been accepted for publication.

Accepted Manuscripts are published online shortly after acceptance, before technical editing, formatting and proof reading. Using this free service, authors can make their results available to the community, in citable form, before we publish the edited article. We will replace this *Accepted Manuscript* with the edited and formatted *Advance Article* as soon as it is available.

You can find more information about *Accepted Manuscripts* in the [Information for Authors](#).

Please note that technical editing may introduce minor changes to the text and/or graphics, which may alter content. The journal's standard [Terms & Conditions](#) and the [Ethical guidelines](#) still apply. In no event shall the Royal Society of Chemistry be held responsible for any errors or omissions in this *Accepted Manuscript* or any consequences arising from the use of any information it contains.

Initial Decomposition Reaction of Di-Tetrazine-Tetroxide (DTTO) from Quantum Molecular Dynamics: Implications for a Promising Energetic Material

Cite this: DOI: 10.1039/x0xx00000x

Received 00th January 2012,
Accepted 00th January 2012

DOI: 10.1039/x0xx00000x

www.rsc.org/

Cai-Chao Ye,^{a,b} Qi An,^a William A. Goddard, III,^{*a} Tao Cheng,^a Wei-Guang Liu,^a Sergey V. Zybin^a and Xue-Hai Ju^b

Di-Tetrazine-Tetroxide (DTTO) was predicted in 2001 to have a density (up to 2.3 g/cc) and heat of detonation (up to 421.0 kcal/mol) better than other explosives, making it the “holy grail” of energetic materials (EMs), but all attempts at synthesis have failed. We report Density Functional Theory (DFT) molecular dynamics simulations (DFT-MD) on DTTO crystal for the two most stable monomers. We predict that the most stable isomer (c1) has a density of $\rho = 1.96$ g/cc with an estimated detonation velocity (D_v) of 9.70 km/s and a detonation pressure (D_p) of 43.0 GPa, making it comparable to RDX ($\rho = 1.82$ g/cc, $D_v = 8.75$ km/s, $D_p = 35.0$ GPa), HMX ($\rho = 1.91$ g/cc, $D_v = 9.10$ km/s, $D_p = 39.3$ GPa) and CL-20 ($\rho = 2.04$ g/cc, $D_v = 9.38$ km/s, $D_p = 44.1$ GPa). The DFT-MD studies find that the initial reaction at lower pressure is unimolecular decomposition to form two N_2O molecules (barrier 45.9 kcal/mol), while at higher pressure it is intermolecular oxygen-transfer with a barrier of 40.1 kcal/mol. For the c2 isomer (less stable by 1.2 kcal/mol) the initial reaction involves two DTTO molecules reacting to form a dimer which then releases N_2 as a direct product (barrier 48.1 kcal/mol), a unique initial reaction among EMs. These results suggest that DTTO may have a higher thermal stability (barrier >7.0 kcal/mol higher) than RDX, HMX, and CL-20.

1. Introduction

The last decade has seen tremendous progress in using quantum mechanics (QM) to predict the detailed reaction barriers and kinetics of gas phase bimolecular and unimolecular reactions with detailed confirmation from experiment and concomitant interpretation of experiment¹⁻⁹. In addition, the last few years has seen similar progress in predicting and explaining the detailed reaction mechanisms, selectivity, and activity of organometallic reactions in solvents that have guided experiment and been confirmed by experiment¹⁰⁻¹³. There has also been significant progress in explaining key aspects of heterogeneous catalysts that have helped somewhat with guiding experiment with some confirmation from experiment¹⁴⁻¹⁶. However, progress has been much more limited in bulk phase reaction mechanisms, where the presence of nearby molecules makes it difficult to distinguish unimolecular from bimolecular processes and experimental interpretations of the initial events seem hopeless because the observed products may be the result of several sequential steps.

This paper is aimed at addressing this issue of determining the initial steps of solid phase reactions. We chose here to examine an energetic material since such systems are much easier to initiate experimentally, making it more likely that an experimentalist might be able to test our predictions. Our previous studies of bulk phase

reactions used the ReaxFF reactive force field to follow the details of the reaction sequences at realistic reaction temperatures and pressures^{4, 17-20}. Indeed, these studies have received some overall confirmation from experiment, but only quantum mechanics (QM) can provide the full detailed mechanistic understanding of the initial reaction steps.

Thus, we report here Density Function Theory (DFT) studies of Di-Tetrazine-Tetroxide (DTTO) crystals, an energetic material that has long been the target of synthetic attempts, because it was estimated to have a high density (up to 2.3 g/cc) and a performance substantially better than traditional EMs (such as RDX, HMX and CL-20), DTTO was seen as the performance limit for CHNO explosives, making it a ‘holy grail’ in high-energy materials.

Previous first principles calculations used plane wave LDA density functional theory²² to predict the most stable isomers of DTTO and the most favorable crystal packing mode. This led to a density of 2.0–2.3 g/cc and a velocity of detonation of $D_v = 10.9$ km/s confirming expectations that DTTO would be a high performance EM, in comparison $D_v = 8.75$ km/s for RDX, $D_v = 9.10$ km/s for HMX, and $D_v = 9.38$ km/s for CL-20.²¹⁻²⁴ However LDA is not reliable for energies of molecular crystals²⁵. So we report here studies using Density Functional Theory (DFT) at various levels (M06, B3LYP, PBE-ulg) which was used to examine the 20 possible

isomers of DTTO. Then Monte Carlo sampling combined with UFF and Dreiding classical force fields was used to predict the best packings (i.e. polymorphs) among the 10 most common space groups for the two most stable isomers, c1 and c2. This was followed by DFT calculations at the PBE-ulg level to optimize the crystal packing²⁶. We found that the most stable isomer c1 has the P212121 space group with 4 molecules per cell (Fig. 1a), leading to a 1.96 g/cc density and a 301.9 kcal/mol detonation enthalpy (393.2 kcal/mol in ref. 23). The c2 isomer (less stable by 1.2 kcal/mol) has the Pbc_a space group with 8 molecules per cell (Fig. 1b) with a 1.98 g/cc density and a 302.4 kcal/mol (393.4 kcal/mol in ref. 23) detonation enthalpy.

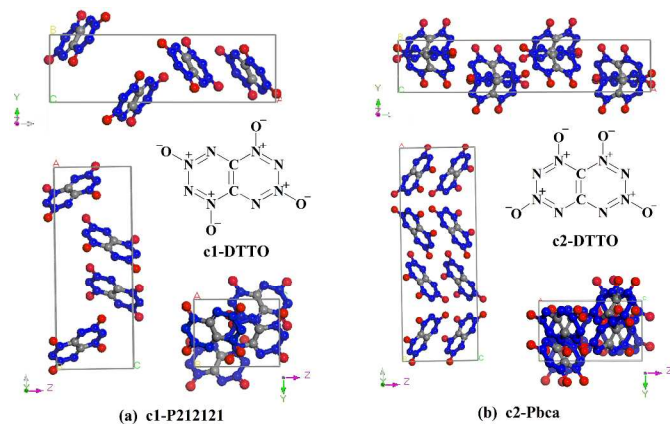


Figure 1 Most stable Molecular isomers Di-Tetrazine-Tetroxide (DTTO), c1 and c2, and their predicted crystal structures: P212121 for c1- and Pbc_a for c2- predicted from previous DFT calculations^{22, 26}. The C, O, N are represented by grey, red, and blue balls, respectively.

In order to determine the energy release, detonation properties, and thermal stability of EMs, it is essential to determine the reaction mechanism for the initial reactions leading to thermal decomposition,^{4, 17, 27-31}. For such nitro-based EMs as TNT, RDX, and HMX the initial decomposition at low pressure is unimolecular NO₂ cleavage³²⁻³⁶. However for hydrogen containing high energetic materials such as RDX and HMX, Chakraborty et al^{3, 27, 31} used DFT to show that intramolecular hydrogen transfer to form HONO provides a complete first step of decomposition³⁷⁻⁴⁰ that dominates under high impact conditions⁴¹. Since DTTO has no hydrogen available to form HONO, its decomposition properties should be dramatically different (maybe better) than normal nitro-based explosives.

In this paper, we report the initial decomposition reaction mechanisms of DTTO using molecular dynamics simulations based on the PBE-ulg⁴² flavor of DFT. The PBE-ulg corrects the poor description of van der Waals attraction (London dispersion) in PBE⁴². Here we consider stable monomers, c1 and c2 starting with their predicted most stable crystal structures (P212121 for c1 and Pbc_a for c2).

2. Simulations and Computational Method

In these DFT based molecular dynamics (MD) simulations, the interatomic forces are calculated in the framework of DFT^{43, 44}, where exchange and correlation were treated with the generalized gradient approximation (GGA), using the functional form of PBE-ulg method⁴².

The condensed phase DFT calculations were performed using VASP package⁴⁵⁻⁴⁸. For structure optimization we found that a kinetic energy cut-off of 500 eV for the plane wave expansions gives excellent convergence of the total energies, energy differences, and structural parameters. The same energy cut-offs were used in the DFT-MD calculations. Reciprocal space was sampled using the Γ -centered Monkhorst-Pack scheme using only the gamma point for the supercell calculations. The convergence criteria were set to a 1×10^{-6} eV energy difference for solving the electronic wave function and a 1×10^{-3} eV/Å force for geometry optimization. They were set to 1×10^{-5} eV energy difference for solving the electronic wave function and a 1×10^{-3} eV/Å force for DFT-MD simulation.

Two DTTO crystalline (c1-P212121 and c2-Pbc_a) phases were considered in the DFT-MD simulations. Both consist of 16 molecules and were obtained by replicating the unit cell twice along the y and z directions for c1-P212121, and twice along the y direction for c2-Pbc_a, respectively. Then the structures for the supercells were optimized individually before molecule dynamics simulations. The two initial structures of c1-P212121 and c2-Pbc_a supercell are shown in Figure S1.

The procedure for the DFT-MD simulations was as follows: First the systems were heated from 20 K to 300 K over a period of 2 ps and then equilibrated at 300 K for 1 ps using the NVT (constant volume, constant temperature and constant number of atoms) ensemble. Finally, we heated the system from 300 K to 3000 K uniformly over the period of 20 ps. The time constant for the Nose-Hoover thermostat was 0.1 ps. We used a time step of 1 fs for integrating the equations of motion. To analyze the fragments during the simulation, we used a bond length cut-off of 1.5 times of the normal bond length. The actual bond lengths cut-offs are shown in the Table S1.

To analyze the mechanisms for the reactions discovered during the simulations, we extracted the molecules undergoing a reaction from the DFT-MD trajectories and then carried out free molecule calculations to locate the nearby transition state for gas phase reactions at the level of PBE-ulg/6-31++G**. The Transition states (TS) were validated to have only one negative eigenvalue for Hessian. This was followed by intrinsic reaction coordinate (IRC) scans to connect the nearby reactant and the product structures⁴⁹. To obtain free energies, we evaluated the thermodynamic properties were at 298.15 K and 1 atm. All gas phase calculations were carried out using the Jaguar 8.2 package⁵⁰.

3. Results and Discussion

The first-principle molecular dynamic simulation in this paper provides a very detailed, molecular-level description of the decomposition and reaction of DTTO in condensed phases under various conditions. Such information should allow one to extract valuable information about the complex chemistry involved, including uni- and multi-molecular reactions¹⁷. Our goal is to elucidate the initial reaction pathway as DTTO decompose and describe the events in this 'holy grail' of high-energy materials as it evolves to form intermediates that react with each other and with reactant to form eventually the final products observed theoretically. In this work, we focus on thermal decomposition of two most stable predicted DTTO crystals, c1-P212121 and c2-Pbc_a, and examine the initial reaction details under various conditions.

3.1 Non-compressed c1-P212121 DTTO

We first examined the initial decomposition reaction of c1-P212121 DTTO. Figure S1 shows the simulated system, which consists of 16 c1-DTTO molecules (224 atoms) in an $18.13 \text{ \AA} \times 10.80 \text{ \AA} \times 13.87 \text{ \AA}$ supercell.

The details of the DFT-MD studies are described below. Briefly we first equilibrate the structure at 300K and then heat it at a uniform rate from 300K to 3000K over 20ps. In our short time simulations (20 ps), no DTTO molecules decompose below 2000 K. Using the same computation approach (heating from 300 K to 3000 K over 20 ps) the decomposition temperature for *beta*-HMX is $\sim 1850 \text{ K}$. This can be compared to the experimental thermal decomposition temperature for HMX of 548 K²⁴. Based on this comparison, we estimate that the experimental thermal decomposition temperature for c1-P212121 DTTO is $\sim 615 \text{ K}$ (similarly the results below suggest that for c2-Pbca the decomposition temperature is 790 K).

As shown in Figure 2(a), for c1-DTTO we found that the first reaction at $\sim 13.2 \text{ ps}$ ($T = 2100 \text{ K}$) is a unimolecular fragmentation of one DTTO molecule to form two N_2O molecules. About 0.1 ps later, additional DTTO molecules decompose, leading to the release of additional N_2O molecules.

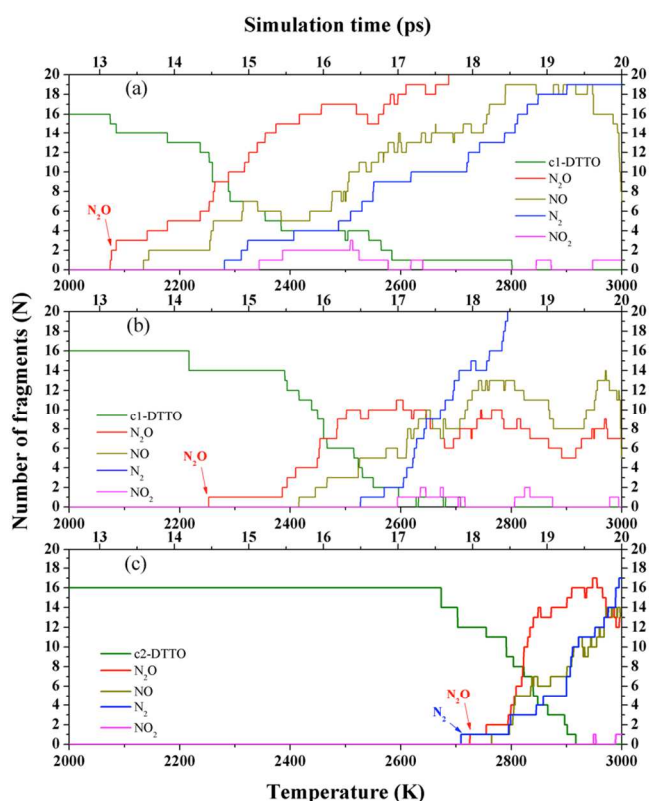


Figure 2. Species analyses for the decomposition of (a) c1-P212121 DTTO heated from 300 to 3000 K over 20 ps. At $\sim 13.2 \text{ ps}$ ($T = 2100 \text{ K}$), the first DTTO molecule decomposes, releasing N_2O molecule. Starting $\sim 0.1 \text{ ps}$ later, DTTO molecules decompose one by one, releasing more N_2O molecules. (b) 30% uniaxial compressed c1-P212121 DTTO is heated from 300 to 3000 K over 20 ps. At $\sim 14.2 \text{ ps}$ ($T = 2250 \text{ K}$), two DTTO molecules react, to yield one N_2O product. At about 15.5 ps ($T = \sim 2400 \text{ K}$), DTTO molecules start decomposing one by one, producing more N_2O molecules are also produced one by one (c) c2-Pbca DTTO heated from 300 to 3000 K over 20 ps. At $\sim 17.5 \text{ ps}$ ($T = 2670 \text{ K}$), two DTTO molecules combine and 0.4 ps later, at $\sim 17.9 \text{ ps}$ ($T = 2700 \text{ K}$), one N_2 molecule is released. At $T = \sim 2700 \text{ K}$, one N_2O molecules was released.

To understand the nature of this first reaction of c1-P212121 DTTO at $\sim 13.2 \text{ ps}$ ($T = \sim 2100 \text{ K}$), we extracted the activated intermediate from the condensed phase simulation and analyzed the reaction mechanism as a gas phase unimolecular reaction. As described below we found the nearby transition state (TS) that has a single saddle point and then minimized to find the nearby stable reactant and product species. The observed reactions and the enthalpy of each species calculated in gas phase are shown in Figure 3 and discussed below in detail.

We find that the unimolecular decomposition starts with breaking N-N and C-N bonds simultaneously to release the first N_2O via TS1 with a 45.9 kcal/mol barrier. As the first N_2O leaves, the adjacent C forms a triple bond with its only neighbor N atom, driving the remaining 6-member ring to open to the intermediate **b** with 7.2 kcal/mol exothermicity. In this N_2O dissociation reaction, the $p\pi$ orbitals in resonance on O and N become singly-occupied sp^2 orbitals, resulting in a lone-pair on N and an N=O double bond, as illustrated in the sub-view of Figure 3. This mode of electron flow from π to σ is commonly observed in dissociation of N_2O from EMs, such as RDX or HMX^{27,31}.

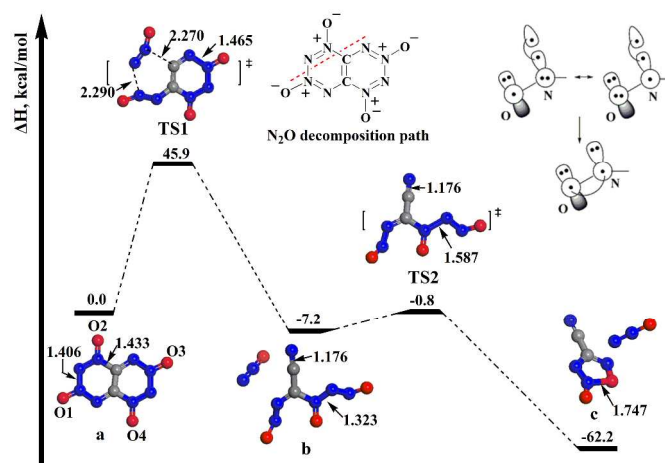


Figure 3. Mechanism of c1-DTTO unimolecular decomposition obtained from gas phase calculations starting from the reactive intermediate extracted from the DFT-MD trajectory. This leads to release of two N_2O molecules. Configurations TS1, TS2 and **c** are obtained from finite cluster DFT calculations.

The next reactive step is to break the N-N bond via TS2 to release the second N_2O with only a 6.4 kcal/mol barrier, leading to ring-closure with very high exothermicity (-55.0 kcal/mol from **b**). This is much greater than the -7.2 kcal/mol exothermicity of the first N_2O reaction that drives further decomposition of other DTTO.

3.2 Compressed c1-P212121 DTTO

It is generally accepted that the detonation starts at a hotspot that forms as the shock wave passes through⁵¹⁻⁵³. Thus we also examined the mechanism of the initial reaction of c1-P212121 DTTO compressed by 30% along the *a* direction (from *a* lattice constant of 18.13 \AA to 12.69 \AA) as shown in Figure 4. This pre-compression leads to an initial external pressure of 15.9 GPa. Then we built a $1 \times 2 \times 2$ supercell containing 16 molecules and 224 atoms, as shown in Figure S1(b). Next we carried out DFT-MD as above, leading to the results in Figure 2(b). Here the c1-DTTO

molecules start to react at ~ 14.2 ps ($T = 2250$ K), with two DTTO molecules reacting to form new covalent bonds while releasing one N_2O product. Thus the initial reaction in the compressed system is not unimolecular.

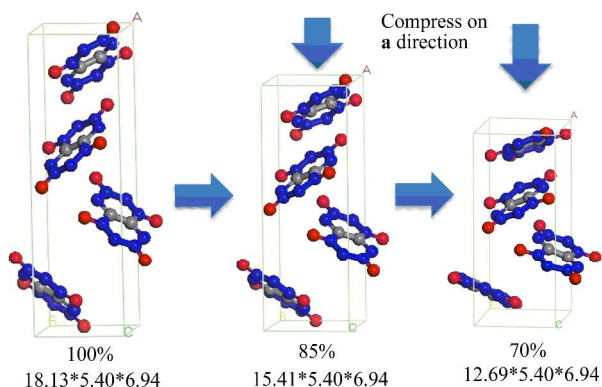


Figure 4. Later view of 30% volume compression in *a* direction of c1-P212121 DTTO unit cell. First compress the unit cell 15% and then go on compress it to 30%. Lattice constants are in Å.

Analyzing the reaction mechanism for just the bimolecular reaction of compressed c1-P212121 DTTO, we found that this first reaction starts an oxygen-transfer between the two adjacent DTTO molecules, which is quite different from the mechanism in RDX and HMX EMs in which hydrogen-transfer to form HONO takes places at the beginning^{27, 54, 55}.

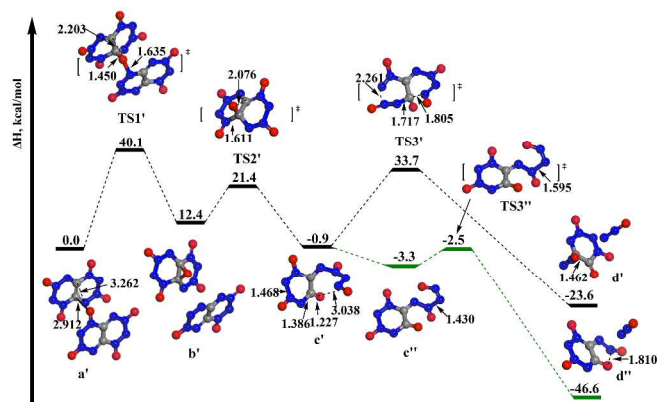


Figure 5. The mechanism of the first bimolecular reaction for compressed c1-DTTO. First there is oxygen-transfer between the two DTTO molecules, which is followed quickly by N_2O release. Configurations $TS1'$, $TS2'$ and $TS3'$ were extracted from the DFT-MD trajectory and then optimized as a gas phase reaction. Path c'' - $TS3''$ - d'' releases one N_2O , but was not observed in the DFT-MD simulations, we find a negligible barrier in the gas phase. The energies for these species involved in the decomposition sequence were calculated by finite cluster DFT calculations.

As shown in Figure 5, this bimolecular reaction involves three steps. The first step is the oxygen-transfer to make DTTO-epoxide via $TS1'$, in which one oxygen atom of c1-DTTO reacts with the C atom of the nearby DTTO to make the first C-O bond, followed by breaking the N-O bond and formation of the epoxide intermediate b' . This reaction is the rate-determining step (RDS) with a 40.1 kcal/mol barrier, which is 5.8 kcal/mol lower than the unimolecular N_2O -release reaction in uncompressed c1-P212121 DTTO.

The second step starts with the ring-opening reaction of the epoxide ($TS2'$), which then form a new C=O double bond that drives the opening of the other 6-member ring to the intermediate c' . This reaction has a 9.0 kcal/mol barrier and releases an enthalpy of 13.3 kcal/mol. The third step to release N_2O observed in the MD simulation is via an S_N2 -like mechanism in which the previously opened branch bounces back to form a 6-membered ring while releasing the N_2O on the other side, leading to a 34.6 kcal/mol barrier but with an exothermicity of 22.7 kcal/mol from c' . Starting with intermediate c' , we find a negligible barrier to first twist the opened branch and then stretch the N-N bond via $TS3''$. Despite the low gas phase barrier, this twist motion of the opened branch takes considerable free space so that it would be hindered by nearby DTTO molecules in the condensed phase, explaining why it was not observed in the MD simulation with its fast heating rate.

After the initial reaction at 14.2 ps, we found that at 15.5 ps ($T = 2400$ K), a number of N_2O molecules are released via unimolecular pathways, while the number of intact c1-DTTO molecules decreases one by one as shown in Figure 6. This N_2O elimination is via $TS4'$ at 43.3 kcal/mol, which gives a heterobicyclic ring f' with reaction enthalpy of -23.9 kcal/mol.

For c1-DTTO, we find a different reaction mechanism for the non-compressed state compared to the highly compressed state. For compressed c1-DTTO, the initial reaction involves an intermolecular oxygen migration, not the unimolecular reaction to release N_2O found for the non-compressed state. This oxygen migration reaction for the compressed case has a reaction barrier 5.8 kcal/mol lower than the N_2O releasing reaction. This result suggests that external shock compression can affect on the decomposition pathway of energetic materials.

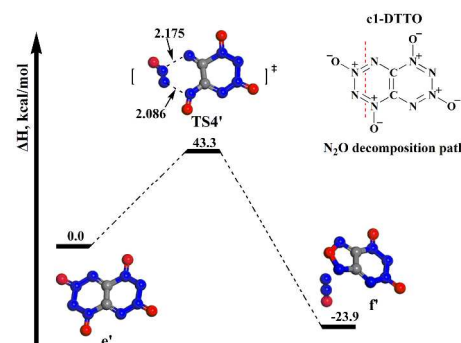


Figure 6. Proposed mechanism of the N_2O elimination reaction in one c1-DTTO molecule. Configurations $TS4'$ and f' are revealed by QM molecular dynamic simulations, and calculate accurate energies for these species involved in the decomposition sequence by DFT calculations.

3.3 Non-compressed c2-Pbca DTTO

We then examined the initial decomposition mechanism for the c2 molecular isomer, which has the Pbca space group. Figure 2(c) shows the number of N_2O , NO, N_2 , and NO_2 fragments observed at temperatures ranging from 2000 K to 3000 K (no DTTO molecules decompose below 2000 K), corresponding to 16 ps to 20 ps.

For c2-DTTO we found that the first reactions start at 2670 K (~ 17.5 ps), involving the intermolecular reaction of two c2 molecules, with no gas products released. Then about 0.4 ps later, at ~ 17.9 ps ($T = 2700$ K), one N_2 molecule is released from this bimolecular complex. About 0.1 ps later ($T = \sim 2700$ K), one N_2O molecule was also released. This shows that by 2700 K, the primary

reactions involve both N_2 and N_2O releasing processes. This is quite different from the c1 reaction mechanisms, in which the initial reactions involve unimolecular decomposition or oxygen transfer.

Using QM we analyzed the reaction mechanism for the c2-DTTO bimolecular combination reaction at ~ 17.5 ps (~ 2600 K). As for the c1 case we searched first for the nearby transition state and then minimized to find the stable reactant and product structures. We find that first an N-N bond is formed between the two reacted DTTO molecules and then a new intermediate product appears. As the reaction proceeds, another N-N bond is broken in the newly formed intermediate leading to two new fragments. Then a C-N bond breaks in one of the newly formed fragments, releasing N_2 , while simultaneously an N_2O molecule is released in a unimolecular reaction. The mechanism derived including the enthalpy for each species is shown in Figure 7 for the case of N_2 releasing reaction and in Figure 8 for the case of N_2O releasing reaction.

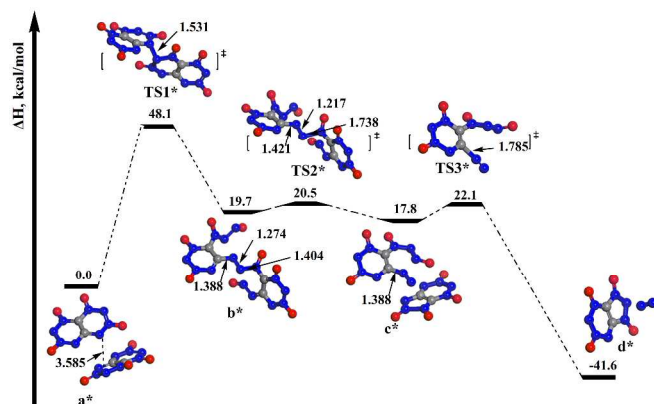


Figure 7. Mechanism from QM molecular dynamic simulations by which two c2-DTTO molecules combine to release N_2 . Configurations $TS1^*$, $TS2^*$, c^* and d^* start with are from by QM molecular dynamic simulations, and calculate accurate energies for these species involved in the decomposition sequence by DFT calculations.

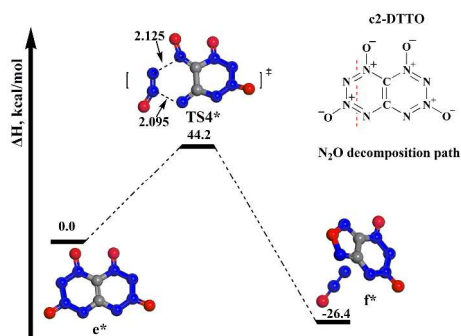


Figure 8. Proposed mechanism of the N_2O elimination reaction in one c2-DTTO molecule. Configurations $TS4^*$ and f^* are revealed by QM molecular dynamic simulations, and calculate accurate energies for these species involved in the decomposition sequence by DFT calculations.

As shown in Figure 7, this N_2 releasing mechanism also involves three steps. The first step is to form an N-N bond between two c2-DTTO molecules via $TS1^*$ with a 48.1 kcal/mol barrier, making it the rate determining step. This reaction opens a 6-member ring on each DTTO leading to a dimer b^* connected with an azo bridge that is 19.7 kcal/mol endothermic. The azo group is then released from the DTTO dimer as a free N_2 by breaking N-N and N-

C bonds sequentially via $TS2^*$ and $TS3^*$ with low barriers (<5 kcal/mol) to the product d^* . This very exothermic reaction ($\Delta H = -41.6$ kcal/mol versus a^*) leads to the decomposition of other DTTO molecules, just 0.1 ps after the first reaction, with one N_2O molecules released. As shown in Figure 8, this N_2O elimination proceeds via $TS4^*$ with 44.2 kcal/mol, which similar to the N_2O elimination reaction shown in Figure 6 except for the position of the breaking bonds.

4. Conclusions

In summary, these DFT molecular dynamics simulations provide a very detailed, molecular-level description of the initial decompositions and reactions of condensed phase DTTO under various conditions. This allows information about the complex chemistry involved to be extracted, including unimolecular and multimolecular reactions sequences¹⁷.

The goal in this paper was to examine the initial reaction pathway as DTTO decomposes to discover the events in this 'nitrogen-rich energetic material' as it evolves to form intermediates that react with each other and with reactant to eventually form the final products observed theoretically and experimentally.

We found three major initial reaction routes, depending upon temperature, pressure, and crystalline structure conditions:

- (1) The first decomposition reaction of uncompressed c1-P212121 DTTO is a unimolecular reaction that releases two N_2O molecules, with an enthalpic barrier of 45.9 kcal/mol and an exothermicity of 6.4 kcal/mol (PBE-ulg).
- (2) As c1-P212121 DTTO is compressed, the initial reaction becomes intermolecular transfer an oxygen atom from one c1 molecule to the nearest carbon of another, leading to an enthalpic barrier of 40.1 kcal/mol.
- (3) For c2-Pbca DTTO, the decomposition reaction mechanism involves first combining two DTTO molecules and then releasing an N_2 molecule, leading to a reaction barrier of 48.1 kcal/mol.

These results suggest that a variety of initial decomposition reactions are favorable for DTTO, depending on temperature, pressure, and crystal packing. The c2-Pbca DTTO reaction begins at 300 K higher than c1-P212121 but leads to bimolecular N_2 release, of twice the energy as for the unimolecular N_2O releasing reaction. This suggests that the thermal stability for c2-Pbca DTTO is higher than for c1-P212121 DTTO. Thus the c2-Pbca could have better performance than c1 DTTO crystal.

The reaction barriers of 45.9 kcal/mol and 48.1 kcal/mol found for c1 and c2 DTTO are higher than the 39.0 kcal/mol NO_2 dissociation barrier for RDX, the 39.8 kcal/mol NO_2 dissociation barrier of for HMX and the 37.6 kcal/mol N- NO_2 homolysis reaction barrier of CL-20^{27, 31, 56}, and the simulated initial decomposition temperatures are 200K or more higher than beta-HMX by the same computational method. Thus we expect that DTTO may be a high performance explosive with higher thermal stability.

We expect these theoretical studies of the initial reaction of DTTO might stimulate further experimental studies of DTTO, particularly the synthesis, and characterization.

Acknowledgements

We thank Dr. Cliff Bedford and Dr. Al Stern for suggesting the importance of this work. All computations were carried out on the Army HPC systems; we thank Betsy Rice and Larry Davis for assistance. Personnel were supported mostly by ONR (N00014-09-1-0634, Cliff Bedford), with some assistance from ARO (W911NF-05-1-0345 and W911NF-08-1-0124). C.-C. Ye was sponsored by the China Scholarship Council (CSC), and thanks the Innovation Project for Postgraduates in Universities of Jiangsu Province (Grant No. CXZZ13_0213).

Notes and references

^a Materials and Process Simulation Center, California Institute of Technology, Pasadena, California 91125, United States.

^b Key Laboratory of Soft Chemistry and Functional Materials of MOE, School of Chemical Engineering, Nanjing University of Science and Technology, Nanjing 210094, P. R. China

* Corresponding author: email: wag@wag.caltech.edu.

† Electronic Supplementary Information (ESI) available: Coordinates for structure of c1-P212121 and c2-Pbca DTTO, studied supercell of c1-P212121 DTTO and c2-Pbca DTTO, and atomic coordinates of all intermediates and TS shown in this study. See DOI: 10.1039/b000000x/

- H. Xiao, Q. An, W. A. Goddard III, W. G. Liu and S. V. Zybin, *P. Natl. Acad. Sci. USA*, 2013, **110**, 5321-5325.
- A. Hammerl, T. M. Klapotke, H. Noth, M. Warchhold, G. Holl, M. Kaiser and U. Ticmanis, *Inorg. Chem.*, 2001, **40**, 3570-3575.
- D. Chakraborty, R. P. Muller, S. Dasgupta and W. A. Goddard III, *J. Comput.-Aided Mater.*, 2002, **8**, 203-212.
- A. Strachan, E. M. Kober, A. C. van Duin, J. Oxgaard and W. A. Goddard III, *J. Chem. Phys.*, 2005, **122**, 54502.
- W. G. Liu, S. Q. Wang, S. Dasgupta, S. T. Thynell, W. A. Goddard III, S. Zybin and R. A. Yetter, *Combust. Flame*, 2013, **160**, 970-981.
- O. Bolton and A. J. Matzger, *Angew. Chem. Int. Edit.*, 2011, **50**, 8960-8963.
- D. C. Clary, *P. Natl. Acad. Sci. USA*, 2008, **105**, 12649-12653.
- M. L. McKee, H. P. Reisenauer and P. R. Schreiner, *J. Phys. Chem. A*, 2014, **118**, 2801-2809.
- R. T. Skodje, *Adv. Quantum. Chem.*, 2012, **63**, 119-163.
- L. D. McPherson, M. Drees, S. I. Khan, T. Strassner and M. M. Abu-Omar, *Inorg. Chem.*, 2004, **43**, 4036-4050.
- D. R. Kent, N. Dey, F. Davidon, F. Gregoire, K. A. Petterson, W. A. Goddard III and J. D. Roberts, *J. Am. Chem. Soc.*, 2002, **124**, 9318-9322.
- D. R. Kent, K. A. Petterson, F. Gregoire, E. Snyder-Frey, L. J. Hanely, R. P. Muller, W. A. Goddard III and J. D. Roberts, *J. Am. Chem. Soc.*, 2002, **124**, 4481-4486.
- V. R. Ziatdinov, J. Oxgaard, O. A. Mironov, K. J. H. Young, W. A. Goddard III and R. A. Periana, *J. Am. Chem. Soc.*, 2006, **128**, 7404-7405.
- O. A. Mironov, S. M. Bischof, M. M. Konnick, B. G. Hashiguchi, V. R. Ziatdinov, W. A. Goddard III, M. Ahlquist and R. A. Periana, *J. Am. Chem. Soc.*, 2013, **135**, 14644-14658.
- A. V. Sbergaeva, W. G. Liu, R. J. Nielsen, W. A. Goddard III and A. N. Vedernikov, *J. Am. Chem. Soc.*, 2014, **136**, 4761-4768.
- W. G. Liu, A. V. Sbergaeva, R. J. Nielsen, W. A. Goddard III and A. N. Vedernikov, *J. Am. Chem. Soc.*, 2014, **136**, 2335-2341.
- S. P. Han, A. C. van Duin, W. A. Goddard III and A. Strachan, *J. Phys. Chem. B*, 2011, **115**, 6534-6540.
- N. Rom, B. Hirshberg, Y. Zeiri, D. Furman, S. V. Zybin, W. A. Goddard III and R. Kosloff, *J. Phys. Chem. C*, 2013, **117**, 21043-21054.
- L. C. Liu, C. Bai, H. Sun and W. A. Goddard III, *J. Phys. Chem. A*, 2011, **115**, 4941-4950.
- L. Z. Zhang, S. V. Zybin, A. C. T. van Duin, S. Dasgupta, W. A. Goddard III and E. M. Kober, *J. Phys. Chem. A*, 2009, **113**, 10619-10640.
- H. Östmark, S. Wallin and P. Goede, *Cent. Eur. J. Energ. Mater.*, 2007, **4**, 83-108.
- X. L. Song, J. C. Li, H. Hou and B. S. Wang, *J. Comput. Chem.*, 2009, **30**, 1816-1820.
- P. Politzer, P. Lane and J. S. Murray, *Cent. Eur. J. Energ. Mater.*, 2013, **10**, 37-52.
- D. Klasovity, S. Zeman, A. Ruzicka, M. Jungova and M. Rohac, *J. Hazard. Mater.*, 2009, **164**, 954-961.
- K. R. Jorgensen and A. K. Wilson, *J. Comput. Chem.*, 2012, **33**, 1967-1968.
- J. L. Mendoza-Cortes, Q. An, W. A. Goddard III, C. Ye and S. V. Zybin, *J. Comput. Chem.*, 2014, submitted.
- D. Chakraborty, R. P. Muller, S. Dasgupta and W. A. Goddard III, *J. Phys. Chem. A*, 2000, **104**, 2261-2272.
- N. Umezawa, R. K. Kalia, A. Nakano, P. Vashista and F. Shimojo, *J. Chem. Phys.*, 2007, **126**, 234702.
- R. A. Fifer, in *Fundamentals of Solid-Propellant Combustion*, AIAA, New York, 1984.
- M. R. Manaa, L. E. Fried, C. F. Melius, M. Elstner and T. Frauenheim, *J. Phys. Chem. A*, 2002, **106**, 9024-9029.
- D. Chakraborty, R. P. Muller, S. Dasgupta and W. A. Goddard III, *J. Phys. Chem. A*, 2001, **105**, 1302-1314.
- S. N. Bulusu, in *Chemistry and physics of energetic materials*, Kluwer Academic, Boston Norwell, MA, U.S.A., 1990.
- C. J. Wu and L. E. Fried, *J. Phys. Chem. A*, 1997, **101**, 8675-8679.
- K. K. Irikura, *J. Phys. Chem. A*, 2013, **117**, 2233-2241.
- R. Cohen, Y. Zeiri, E. Wurzburg and R. Kosloff, *J. Phys. Chem. A*, 2007, **111**, 11074-11083.
- X. F. Chen, J. F. Liu, Z. H. Meng and K. L. Han, *Theor. Chem. Acc.*, 2010, **127**, 327-344.
- B. Wang, D. Wright, D. Cliffel, R. Haglund and S. T. Pantelides, *J. Phys. Chem. A*, 2011, **115**, 8142-8146.
- D. Furman, R. Kosloff, F. Dubnikova, S. V. Zybin, W. A. Goddard III, N. Rom, B. Hirshberg and Y. Zeiri, *J. Am. Chem. Soc.*, 2014, **136**, 4192-4200.
- C. A. Mayhew, P. Sulzer, F. Petersson, S. Haidacher, A. Jordan, L. Mark, P. Watts and T. D. Mark, *Int. J. Mass. Spectrom.*, 2010, **289**, 58-63.
- Z. Takats, I. Cotte-Rodriguez, N. Talaty, H. W. Chen and R. G. Cooks, *Chem. Commun.*, 2005, 1950-1952.
- A. Strachan, A. C. van Duin, D. Chakraborty, S. Dasgupta and W. A. Goddard III, *Phys. Rev. Lett.*, 2003, **91**, 098301.
- H. Kim, J. M. Choi and W. A. Goddard III, *J. Phys. Chem. Lett.*, 2012, **3**, 360-363.
- W. Kohn and L. J. Sham, *Phys. Rev.*, 1965, **140**, 1133-&.
- P. Hohenberg and W. Kohn, *Phys. Rev. B*, 1964, **136**, B864+.
- G. Kresse, *J. Non-Cryst Solids*, 1995, **193**, 222-229.
- G. Kresse and J. Furthmuller, *Comp. Mater. Sci.*, 1996, **6**, 15-50.
- G. Kresse and J. Furthmuller, *Phys. Rev. B*, 1996, **54**, 11169-11186.
- G. Kresse and D. Joubert, *Phys. Rev. B*, 1999, **59**, 1758-1775.
- X. Kim, *Acc. Chem. Res.*, 1981, **14**, 363-368.
- Jaguar, Schrodinger, LLC: New York, NY, 2013.
- F. P. Bowden and A. D. Yoffe, in *Initiation and Growth of Explosions in Liquids and Solids*, Cambridge University Press, Cambridge, UK, 1952.
- Q. An, S. V. Zybin, W. A. Goddard III, A. Jaramillo-Botero, M. Blanco and S. N. Luo, *Phys. Rev. B*, 2011, **84**.
- Q. An, W. A. Goddard III, S. V. Zybin, A. Jaramillo-Botero and T. T. Zhou, *J. Phys. Chem. C*, 2013, **117**, 26551-26561.
- L. M. Minier, K. R. Brower and J. C. Oxley, *J. Org. Chem.*, 1991, **56**, 3306-3314.
- L. L. Davis and K. R. Brower, *J. Phys. Chem.*, 1996, **100**, 18775-18783.
- S. Okovityy, Y. Kholod, M. Qasim, H. Fredrickson and J. Leszczynski, *J. Phys. Chem. A*, 2005, **109**, 2964-2970.

Table of Contents

A variety of initial decomposition reactions are favorable for DTTO, depending on temperature, pressure, and crystal packing.

